Imaging biological structures with a proton microprobe

Teresa Pinheiro [1,1], Maria Dolores Ynsa [2] and Luís C. Alves [1]

1 - Instituto Tecnológico e Nuclear & Centro de Física Nuclear da Universidade de Lisboa, E.N. 10, 9685 953 Sacavém, Portugal
2 - CMAM, Universidade Autónoma de Madrid, Cantoblanco 28049 Madrid, Spain.

Imaging the morphology of the tissue *in vivo* and producing the correspondent elemental maps, whether in major, minor, or trace concentrations in real-time can be done using a focused beam of accelerated particles. This can be accomplished using different ion beam techniques simultaneously such as Scanning transmission ion microscopy (STIM), secondary electron imaging (SEI), Rutherford backscattering spectrometry (RBS), and particle induced X-ray emission (PIXE). The results are fully quantitative. The experimental set-up including focusing, scanning and detection systems, is often called Nuclear Microprobe, or, if the projectiles are protons, Proton Microprobe. This paper deals with the basic principles of proton microprobe, including data processing and imaging. Considerations for specimen preparation requirements and for interpretation of results are focused. Examples of applications to biology and to human health problems are given.

Keywords: focused ion beams; trace elements; elemental mapping; microanalysis; lung; skin

1. Introduction

Focused ion beam analysis with micrometer spatial resolution was first put into practice in the early 1970s [1]. Since then, the technology of ion beam optics and scanning systems, as well as detection and data acquisition devices have advanced considerably making possible the application of the generally called nuclear microprobes to various fields of science [2,3]. Many of these microprobes associating a package of analytical techniques that provide structural and quantitative elemental analysis of a specimen at the microscopic level were constructed specifically for applications to materials science and biomedicine. Essentially protons have been used as projectiles widely spreading the designation of proton microprobe. Resolutions in the micrometer range are easily achieved in standard equipments. However, the best systems currently available are able to produce spatial resolutions down to a few tenths of nanometers at the specimen [3]. The nuclear microprobe capability of analysing elemental concentration is often compared with electron microprobe X-ray microanalysis, as both approaches provide multielemental detection of cryopreserved material. The immediate difference between them is the achieved spatial resolution. Due to the limitation of the beam dimension, the superimposed information from intra- and extra-cellular compartments diminish the final attainable resolution of nuclear microprobes, while electron microprobes generally have sub-cellular resolution. Nevertheless, in nuclear microprobes, the detection of scattered and transmitted protons, induced X-rays, emitted secondary electrons, among others, can be done simultaneously and the images produced display features of the sample that cannot promptly be imaged by other techniques [4,5]. This capacity derive from the ability of MeV protons to penetrate deep beneath the sample surface (tenth's of micrometers) with low scattering to produce signals from hidden features. Opposite, electrons impinging on the sample are subject to multiple scattering and energy attenuation, producing a significant background of continuous radiation. This means that in elemental analysis for instance, the weak signal of trace elements are hidden in the background what justifies the low sensitivity of electron microprobe when compared to the proton microprobe. The electron microprobe can generally analyse elemental concentrations down to the 200 μg/g and is therefore unable to detect elements occurring at low concentrations in the tissues, such as

[1] Corresponding author: e-mail: murmur@itn.pt, Phone: +351219941525

Ca, Fe and Zn, which are routinely mapped with a nuclear microprobe. However, for elements that occur at even lower concentrations in biological samples, e.g., Ni and Se long acquisition times would be required to provide statistically significant quantitative data.

Proton microprobes are particularly suited when the preservation of the in vivo condition is required. This is the case of the evaluation of tissue features under physiological condition, such as trace element distribution. Earlier studies on human tissues, e.g., skin, arteries, using nuclear microscopy showed discrete variations in elemental concentrations corresponding to different tissue environments [6,7]. Since then, a variety of biological and medical problems have been focused, namely, brain elemental distributions associated to Alzheimer's disease [8], trace element imbalances in bone and endometrium associated to osteoporosis and hormone replacement therapies [9], Fe and Zn involvement in the atheroma evolution [10]. Developments of the proton probe optics enabled a reduction of the beam dimensions and progressively improved image resolution enabling the accurate visualization of tissue morphological details using transmission images. By combining morphological images with elemental distributions important information can be gathered regarding specific cell environments and tissue structures. This paper illustrates the broad applicability of proton microprobe techniques to biomedical problems, where the distribution of elements in tissues may contribute to study physiological conditions, and to help improving the knowledge on human pathogenesis.

2. General principles

2.1 The proton microprobe components

In a nuclear microprobe the ion beams used for analysis are produced in an accelerator. The energy range required in most of the applications, 1 to 3 MeV, means that small accelerators, preferably with a bright ion source, are adequate. The additional components of a nuclear microprobe needed to produce beams focused down to micrometer or sub-micrometer dimensions are: 1) a focusing system that consists of precision collimation slits and magnetic quadrupoles; and 2) a scanning system to raster the beam over the sample as in a scanning electron microscope (Fig. 1). Samples are usually analyzed in vacuum to prevent unacceptable scattering of the primary beam. In a standard microprobe system the spatial resolution of 0.5-1 μm at the specimen is achieved while maintaining the ion current in the order of 100 pA that is useful for elemental analysis. The large scanning range of up to 3 mm improves the imaging capabilities of the system and permits the scanning of a selected region of interest in the sample. The experimental chamber accommodates a sample stage equipped with a x,y,z manipulator for positioning the sample into the focus plane with the help of a microscope, several radiation detectors and a Faraday-cup for beam charge measurements. Detailed information of the system used in this work has been previously described [11] which is essentially illustrated in Fig. 1.

2.2 2D visualisation

To generate maps the detector signals are recorded and each event assigned to a digital x,y positional coordinate. A single map is obtained for the spectral data (X-ray peak area, barrier area, etc.) and for the statistical treatment of the events occurring at each pixel, which are then used to produce quantitative elemental maps. The quantity measured is usually represented by a colour gradient. To integrate this information commercially available computer code are often used [2, 12]. Maps can be generated on-line using qualitative information taken from spectra energy intervals, or off-line if all the events were recorded in an "event-by-event" mode enabling the extraction of energy spectra corresponding to regions of interest in the sample. These regions may refer to the whole image or to parts of the imaged area. Therefore, neighbour regions of a small specimen can be compared. Point analysis is also possible either by selecting independent isolated details or specific transects.

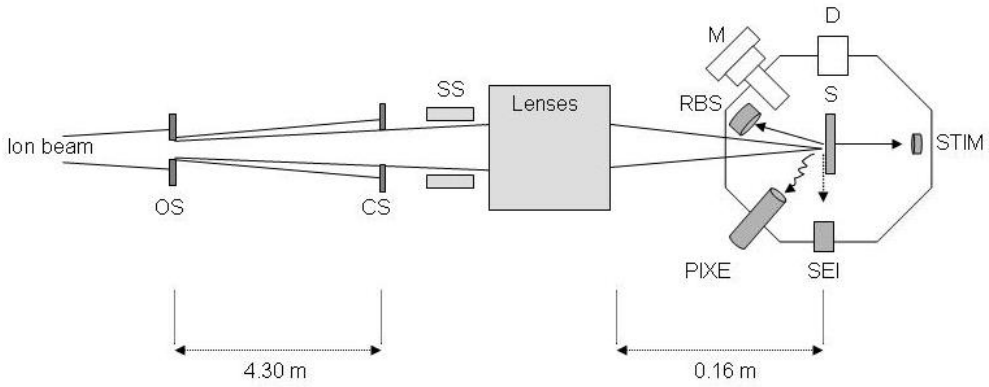

Fig. 1 Lay-out of a nuclear microprobe installed at ITN [11]. H^+ and He^+ beams can be used. The distances between object slits – OS and collimation slits CS and between the focusing lenses system exit and focus plane (S) where the sample is positioned, are given; SS – scanning system for beam deflection. The chamber configuration (Oxford Microbeams Ltd., http://www.microbeams.co.uk) enables a microscope (M) and several detectors for X-rays (PIXE), for backscattered particles (Si surface barrier detector for RBS) for transmitted particles (collimated windowless photodiode for STIM), for secondary electrons (scintillator and photomultiplier system or a channeltron for SEI) and an additional position – D, for other detector.

2.3 Proton microprobe techniques and quantification

The most used techniques in biomedical applications are PIXE (particle induced X-ray emission), RBS (Rutherford backscattering spectrometry, STIM (scanning transmission ion microscopy), and SEI (secondary electron imaging), as they can provide simultaneously morphological and elemental distribution information.

PIXE technique provides minor and trace elemental information. The incoming protons create a inner shell vacancy which will be filled by an electron transition from the outer shell with the emission of an X-ray. The energy of the X-ray is unique to the originating element allowing the elements present in the sample to be identified. The PIXE spectrum enables the simultaneous detection of multiple elements (virtually from Na to U) with excellent quantitative precision and analytical sensitivity (1–10 μg/g on a dry weight basis), especially for transition elements which are the essential trace elements in biological tissues.

RBS is based on the energy of protons that are backscattered from atomic nuclei in the sample and provides information on the matrix composition, e.g., carbon, nitrogen, and oxygen, and on the thickness of the sample. The energy of the backscattered proton depends on the nucleus involved in the collision, thus enabling elemental identification. The energy lost by the proton during its path in and out of the sample enables the measurement of the depth variations. Counting the number of protons backscattered from each element the sample stoichiometry can be determined.

STIM technique enables the analysis of the energy loss of particles across sample for specimen density determinations. The energy loss of the transmitted protons that did not suffer nuclear backscattering collisions is dependent on the density variations of the sample. By measuring density variations, high-resolution images (<0.5μm) of the sample morphology can be obtained routinely. This is particularly helpful in tissue morphology structure as cell boundaries can be identified, if the sample is thin and analysed in self-supported mode.

The combination of PIXE and RBS data allows quantitative measurements of elemental concentrations [13]. Also the density information obtained through the STIM spectra can also be used to normalise PIXE data for quantitative elemental determinations [14,15].

SEI is particularly adequate to thick specimens where STIM cannot be applied. The technique is based on the detection of electrons extracted from the atoms at the sample surface by the incident beam and provides information on sample topography.

2.4 Sample preparation

The sample preparation techniques developed for electron microscopy analysis are generally also applicable in proton microscopy. The method of choice for biomedical materials collected by autopsy or by punch biopsy, involve quench freezing of the specimen in 2-methylbutane cooled in liquid nitrogen, followed by cryosectioning and freeze-drying. Cryosectioning is a critical step in sample preparation, as temperature gradients and sample freezing-out processes may occur when sample is positioned in mounting medium facilitating cell disruption and ion displacement [16,17]. Therefore sections should be obtained from non-immersed tissue parts. Sections of 10-14-μm thick are usually adequate for proton microprobe analysis, as they can be mounted in specific frames in self-supported mode after being allowed to dry inside the cryostat [17]. The thickness of the dry section attained is usually in the 1-2 μm range. The sections can also be mounted on a foil of polycarbonate or silicon nitride adequately thin to enable high-resolution imaging using transmitted ions (STIM). Bulk analysis on thick sections is also possible. This is the case of mineralized tissues, which can be analysed directly or sectioned in an appropriate microtome.

3. Materials and Methods

Trachea, bronchi, lung and lymph nodes samples were taken at autopsy, quench-frozen and sectioned in a cryostat at -25ºC. The sections were mounted on a thin polycarbonate foil and allowed to dry in vacuum. Skin samples were taken by punch biopsy, 3 mm diameter, prepared as indicated above and the cryosections mounted in self supported mode.

The nuclear microprobe installed at ITN Van de Graaff accelerator was used [11]. Samples were irradiated in vacuum with a 2 MeV proton beam of approximately 100 pA. Data was acquired and processed for quantitative analysis with OMDAQ and DAN32 computer codes, respectively [12,13].

4. Results and Discussion

Two categories of applications were selected on the basis of demonstrating the broad applicability of the proton microprobe techniques.

The first example demonstrates the applicability of the proton microprobe to the identification of inhaled particles in the human respiratory system. The tracheal and bronchial mucosas and distal respiratory tissues corresponding to terminal bronchiole and alveoli were inspected for particulate matter deposits. Several particles of 2-15 μm diameters could be detected in the respiratory mucosas. In the overall, it seems that larger particles or larger agglomerations of particles are found in trachea than in bronchi. The deposits in alveoli walls, probably consisting of particles which size is inferior to the spatial resolution of the technique, showed a diffuse pattern in contrast with the well defined boundaries found for particles at upper regions of the respiratory tree (Fig. 2-A and 2-B). Both individual particles and lung deposits likely correspond to inhaled atmospheric dispersed particles. The gradient of particle dimensions found along the respiratory tree is expected if only the aerodynamic properties of particles driven by the air current are taken into account. The elemental compositions determined for particles and deposits consistently associate with those described for particulate matter [18]. High concentrations of Al, Ca and Si were often associated to Cr, Cu, Fe, Ni, Pb and Zn. Clearance processes can also be inferred by mapping the elemental distributions of cortical and medullar regions of lymph nodes that drain respiratory mucosa and of macrophages inclusions. At medullar regions of the lymph nodes, inclusions of about 5 μm were observed associating several elements as depicted in Fig 2-C. These inclusions were probably confined in phagocytic cells [19] that are thought to play some role in the immune response. Macrophage cells, found in the sub-epithelial regions of bronchi and distal pulmonary

tissue, contain dense agglomerates that resemble particles in composition as can be visualised in Fig. 2-D.

The visualisation granted by elemental mapping, the size and elemental composition determined for these particles and the region where they are found in the respiratory system are relevant aspects for environmental health studies.

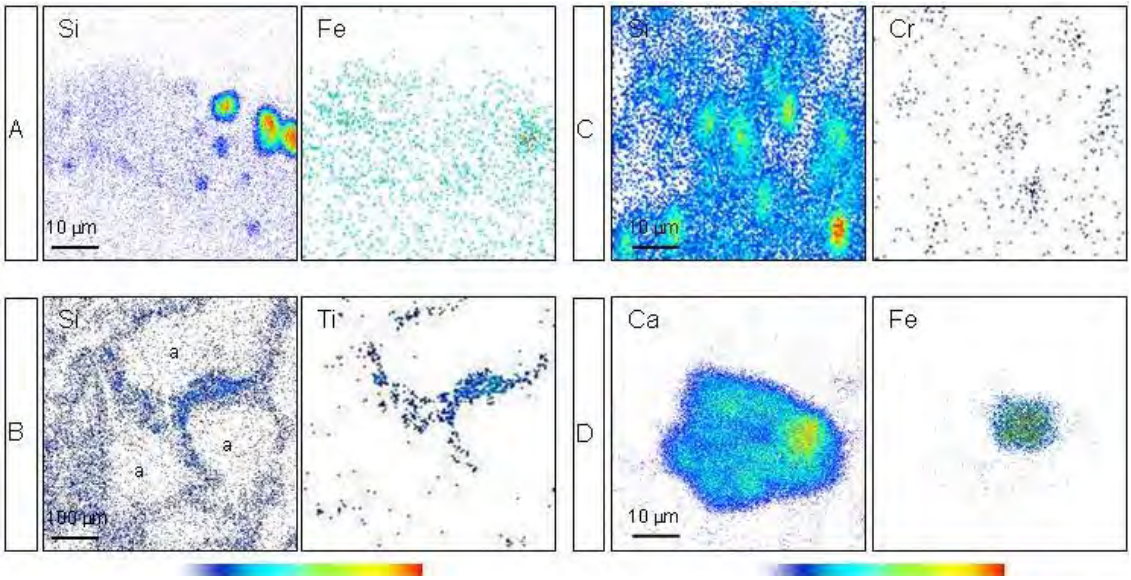

Fig. 2 Images of elemental distributions obtained by PIXE, of 10 µm cryosections of: trachea – A, showing several particles in the mucosa; lung tissue – B, with profuse deposits of Si and Ti at the alveolar walls (a – alveolar space); lymph node medullar regions with inclusions that associate Si and Cr; and a macrophage – D, with several included particles. Contents were plotted on a colour scale as depicted.

The high-resolution imaging provided by STIM in combination with elemental distribution obtained through PIXE and RBS offer information of specific cell environment and tissue structures. The following example demonstrates the unique capability of the proton microprobe to assess percutaneous absorption of products in vivo. Cell layers can be imaged along with concentrations at each layer or at each cell.

High-resolution images of skin were obtained with STIM delivering details on a cell to cell level when small scan areas are performed. Juxtaposed with STIM, RBS and PIXE analysis produce elemental maps of the same scan area. Elemental profiles can be obtained by analysing transects of the inspected area or extracting the information from maps. Therefore the concentrations of the various elements detected can be accurately linked to each skin strata [20]. The distribution, coverage and permeation of nanoparticles of Ti used as physical filter of UV radiation in sunscreens in skin were studied. The Ti distribution is confined to the stratum corneum outer layers, showing no significant penetration in the living cell layers (Fig 3).

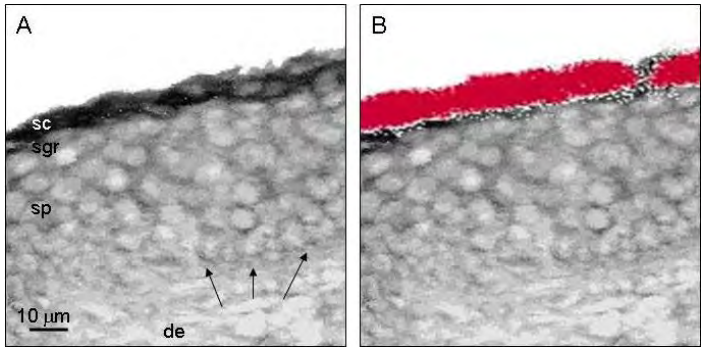

Fig. 3 – Transmission image of a skin section – A (from low density - white, to high density - black). The keratinocyte cells can be identified from stratum germinativum (arrows), all along stratum spinosum – sp, to the statum granulosum (sgr); sc - stratum corneum; de - dermis. The Ti (red) is confined to stratum corneum (sc) as can be observed in B, where density and Ti distribution images are overlapped.

This procedure can be further applied to the study of allergenic interactions with skin and to future studies on trans-epidermal or dermal-delivery of products. A limitation of the method is that the permeating vehicle can only be traceable if the compound contains a metal ion or an element possible to be measured by PIXE.

The same principle can also be used to study skin specific elemental profiles such as Fe in human hemochromatosis. In this genetic disease Fe absorption is not appropriately controlled leading to its accumulation in parenchymal trissues (liver, heart, skin among others) with serious consequences if not treated. It was found that in patients suffering of primary hemochromatosis and at early stages of the disease, Fe consistently deposits in epidermal strata as can be observed in Fig. 4. In addition, the concentration of Fe in epidermis was correlated with the liver Fe deposits [21]. These findings open interesting perspectives for skin, a manageable organ, as an auxiliary tool in the diagnosis of primary and secondary hemochromatosis, and therapy efficacy.

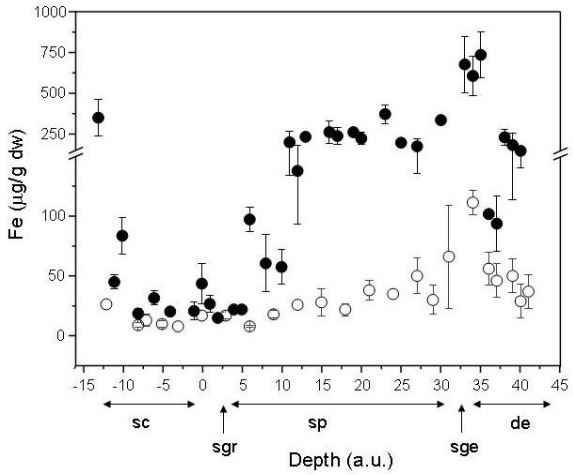

Fig. 4 - Elemental profile of Fe in healthy skin (open circles) and in a patient with hemocromatosis (solid circles) according to distance from the stratum corneum (sc) /stratum granulosum (sgr) interface (zero in the graph) to st. corneum and to living cells strata (st. spinosum – sp, st. germinativum sge, and dermis –de).

5. Final comments

Despite the advantages and disadvantages that can be associated with proton microprobe techniques there are a variety of problems that may profit of their unique characteristics. The reduction of beam dimensions allied to the different charged particles that can be used, paved the way to emerging applications of nuclear microprobes, such as imaging of cells at the nano-level and density tomography [22,23], targeting of single cells and analysis of the induced low-dose radiation damage on a cell-by-cell basis, bystander response and cell communication [24,25].

One of the merits of nuclear microprobes continues to be the outstanding capability to measure trace quantities of elements in cells and tissues. With the development of detectors technology and beam optics the quantitative determination of metals in trace concentrations in vivo, with their eventual

diffusion across tissues and cells, is becoming a feasible task. Metal oxides are widely spread in food and modern hygiene products often with no restrictions to use by consumers. They play a vital role in human physiology although the mechanisms by which they penetrate in the body or induce biological responses are far from being understood. Also, pathological condition can affect imbalances of essential elements. Measuring elemental concentrations in specific tissue environments and individual cells may eventually provide new insights in pathogenesis and cell response mechanisms.

Acknowledgements Authors thank: A. Bugalho de Almeida, R. Silva, R. Fleming, P. Filipe, and J.N. Silva (Sta. Maria Hospital, Lisbon, Portugal); G.W. Grime (Surrey University, England); J. Pallon and K. Malmkvist (Lund University, Sweden) for the fruitful collaboration. Work financed by EC/QLK4-CT-2002-02678, SPDV, FCG/SDH.IC.I.01.22, IAEA 302-F1.20.19-POR-13262.

References

[1] J.A. Cookson, A.T.G. Fergunsen, and F. Pilling, J Radioanal. Chem. **12**,39 (1972).
[2] M.B.H. Breeze, D.N. Jamieson, P.J.C. King. Materials analysis using a nuclear microprobe (John Wiley & Sons, Inc., NY, 1996), pp.428.
[3] ICNMTA2006, Proceedings of the 10th International Conference on Nuclear Microprobe Technology and Applications, 9-14 July Singapore, 2006, in Nucl. Instrum and Methods in Phys. Res. B, doi: 10.1016/j.nimb.2007.03.064.
[4] B. Forslind , M. Lindberg, G.M. Roomans, J. Pallon and Y. Werner-Linde, Microscopy Research Technique **38**, 373 (1997)
[5] J. Pallon, B. Forslind, M. Lindberg. Particle probes and skin physiology. In: Dry skin and mosturizers:chemistry and function, Ed. M. Lodén and H.L. Maibach, 2nd Ed, CRC Press (Taylor & Francis, Boca Raton, 2006), Chp. 5, pp 44-61.
[6] B. Forslind, L. Kunst, K.G. Malmqvist, L.E. Carlsson and G.M. Roomans, Histochemistry **82**, 425 (1985).
[7] J. Pallon, P. Homman, T. Pinheiro, M.J. Halpern, K. Malmqvist, Nucl. Instr. and Meth. in Phys. Res. B **104**, 344 (1995).
[8] J.P. Landsberg, B. McDonald, F. Watt, *Nature* 360, 65 (1992).
[9] M.D. Ynsa, F.J. Ager, L.C. Alves, M.A. Zubeldia, J.C. Millan and T. Pinheiro, J Microsc. **224**, 298 (2006).
[10] M. Ren, R. Rajendran, P. Ning, B. T. K. Huat, O. C. Nam, F. Watt, A. Jenner and B. Halliwell, Free Rad. Biol. Med., 41,222 (2006).
[11] L.C. Alves, M.B.H. Breese, E. Alves, A. Paúl, M.R. da Silva and J.C. Soares, Nucl. Instr. and Meth. in Phys. Res. B **161-163**, 334 (2000).
[12] G.W. Grime and M. Dawson, Nucl. Instr. and Meth. in Phys. Res. B **104**, 107 (1995).
[13] G.W. Grime, Nucl. Instr. and Meth. in Phys. Res. B **109 - 110**, 170 (1996)
[14] J. Pallon, V. Auzelyte, M. Elfman, M. Garmer, P. Kristiansson, K. Malmqvist, C. Nilsson, A. Shariff, M. Wegdén, Nucl. Instrum. Meth. in Phys. Res. B **219-220**,988 (2004).
[15] P. Aguer, L.C. Alves, Ph. Barberet, E. Gontier, S. Incerti, C. Michelet-Habchi, Zs. Kertész, A.Z. Kiss, P. Moretto, J. Pallon, T. Pinheiro, J.-E. Surlève-Bazeille, Z. Szikszai, A. Veríssimo, M.D. Ynsa, Nucl. Instr. and Meth. in Phys. Res. B **231**, 292 (2005).
[16] I. Kozlova and G.M. Roomans, Am. J. Transplant **3**, 697 (2003)
[17] T. Pinheiro, J. Pallon, L.C. Alves, A. Veríssimo, P. Filipe, J.N. Silva and R. Silva, Nucl. Instr. and Meth. in Phys. Res. B (2007), doi: 10.1016/j.nimb.2007.02.014.
[18] T. Pinheiro, L. C. Alves, A. Bugalho de Almeida, M. J. Palhano, E. Pålsgård and G. W. Grime, Nucl. Instr. and Meth. in Phys. Res. B **158**, 499 (1999).
[19] T. Pinheiro, L.C. Alves, M.J. Palhano, and A. Bugalho de Almeida, Nucl. Instr. and Meth. in Phys. Res. B **181**, 499 (2001).
[20] A. Veríssimo, L.C. Alves, P. Filipe, J.N. Silva, R. Silva, M.D. Ynsa, E. Gontier, P. Moretto, J. Pallon, and T. Pinheiro, Microscopy Research and Technique **70**, 302 (2007).
[21] I. Guinote, R. Fleming, R. Silva, P. Filipe, J.N. Silva, A. Veríssimo, P. Napoleão, L.C. Alves and T. Pinheiro, Nucl. Instr. and Meth. in Phys. Res. B **249**, 697 (2006)
[22] R. Minqin, J.A. van Kan, A.A. Bettiol, L. Daina, C. Yee Gek, B. Boon Huat, H.J. Whitlow, T. Osipowicz and F. Watt, Nucl. Instr. and Meth. in Phys. Res. B (2007), doi:10.1016/j.nimb.2007.02.015

[23] C. Habchi, D.T. Nguyen, G. Devès, S. Incerti, L. Lemelle, P. Le Van Vang, Ph. Moretto, R. Ortega, H. Seznec, A. Sakellariou, C. Sergeant, A. Simionovici, M.D. Ynsa, E. Gontier, M. Heiss, T. Pouthier, A. Boudou, F. Rebillat, Nucl. Instr. and Meth. in Phys. Res. B **249**, 653 (2006).
[24] S. Gerardi, Radiat Prot Dosimetry (2006), doi:10.1093/rpd/ncl444.
[25] O.V. Belyakov, S.A. Mitchell, D. Parikh, G. Randers-Pehrson, S.A. Marino, S.A. Amundson, C.R. Geard, and D.J. Brenner, Proc Nat Acad Sc, **102**,14203 (2005)